

Texture Evolution During Laser Direct Metal Deposition of Ti-6Al-4V

NIYANTH SRIDHARAN,^{1,3,4} ANIL CHAUDHARY,²
PEEYUSH NANDWANA,³ and SUDARSANAM SURESH BABU^{1,3}

1.—Department of Mechanical, Aerospace, and Biomedical Engineering, The University of Tennessee, Knoxville, TN 37996, USA. 2.—Applied Optimization, 714 East Monument Avenue, Suite 204, Dayton, OH 45402, USA. 3.—Manufacturing Demonstration Facility, Oak Ridge National Laboratory, Oak Ridge, TN 37831, USA. 4.—e-mail: niyanth.sridharan@gmail.com

Titanium alloys are used in a wide variety of high-performance applications and hence the processing of titanium and the resulting microstructures after additive manufacturing has received significant attention. During additive manufacturing, the processing route involves the transition from a liquid to solid state. The addition of successive layers results in a complex microstructure due to solid-state transformations. The current study focuses on understanding the phase transformations and relate them to the transformation texture in Ti-6Al-4V to identify conditions leading to a strong alpha transformation texture. The as-deposited builds were characterized using optical microscopy and electron backscattered diffraction. The results showed columnar prior β grains with a martensitic structure after the deposition of a single layer. On subsequent depositions, the martensitic microstructure decomposed to a colony and basketweave microstructure with a stronger transformation texture. The alpha texture with a colony and basketweave microstructure showed a stronger transformation texture as a result of variant selection. Thus, by controlling the cooling rate of the build from the β transus, it is possible to control the alpha transformation texture.

INTRODUCTION

Titanium and its alloys are widely used in aerospace applications due to their high strength to weight ratio.¹ In recent years, the fabrication of metallic parts using the solid free form fabrication route has been shown to be promising since cost savings can be realized by repairing and reusing high-value aerospace parts. Laser direct metal deposition (LMD) offers a potential solution by virtue of its low heat input and distortion levels.² However, the repeated heating and cooling cycles cause spatial variations of microstructure and these effects coupled with lack of fusion and porosity defects in the build result in degradation in the high cycle fatigue properties.^{3,4}

Hence, much work has been focused to improve the fatigue properties by microstructure control,^{2,3} alloying,⁵ and defect elimination.⁵ Although significant improvements in the fatigue properties were realized in these studies, there is a need to fabricate

builds with better fatigue properties on par with wrought components. The texture dependence of high cycle fatigue in titanium alloys has been well documented.⁶ The processing route of additive manufacturing involves a complex transition from liquid to the solid state and successive depositions act as heat treatments for the already deposited layers leading to solid-state phase transformations.⁷

Ti-6Al-4V undergoes a solid-state phase transformation during cooling in which the high-temperature β phase transforms to the room-temperature $\alpha + \beta$ phase. During phase transformation, titanium alloys follow a specific Burger's orientation relationship where the $\{110\}_\beta \parallel (0001)_\alpha$ and the $\langle 111 \rangle_\beta \parallel \langle 1120 \rangle_\alpha$. There are three $\langle 1120 \rangle_\alpha$ directions on a $(0001)_\alpha$ plane and two close-packed $\langle 111 \rangle_\beta$ on one $\{110\}_\beta$. Thus, 1 single beta grain can transform to 12 different alpha orientations during cooling.⁸ This would lead to a weak α texture during transformation if all the variants were selected with equal probability,^{9,10} However, that is rarely the case. It

has been demonstrated in numerous studies that the selection of the alpha variant when the beta transforms is not random but is controlled by

- i. The presence of specific grain boundary characteristics in the high-temperature beta,^{8,9,10}
- ii. The self-accommodation of the strains produced during beta to alpha transformation.^{11,10,12}

The selection of specific variants could lead to the formation of a strong α texture. The formation of α transformation texture is dependent on the prior beta grain size,¹³ heating temperature and cooling rate.¹⁰ Texture development of Ti-6Al-4V during electron beam,^{14,15} and laser additive manufacturing⁷ has been studied. All studies confirmed that alpha texture was random. The observed texture was hypothesized to be a result of the lack of variant selection during the phase transformation from the high-temperature β to the room-temperature $\alpha + \beta$ phase. However, there are no studies which have investigated the changes in texture as a function of build height. The aim of this work is to investigate the changes in texture and microstructure as a function of the build height and to identify the conditions which lead to variant selection so as to tailor the texture in the Ti-6Al-4V direct metal deposits to improve the high cycle fatigue properties.

EXPERIMENTAL PROCEDURE

For this study, the Ti-6Al-4V builds were made using PREP powder with a size distribution of 44–120 μm . Four builds with 1, 2, 3 and 4 layers with a layer height of 0.5 mm were made using a laser power of 400 W, a powder feed rate of 2.1 g/min and a scan speed of 25 inches/min (63.5 cm/min) on a DM3D 103D machine. The builds were made on a wrought Ti-6Al-4V substrate. The laser used for deposition was a 1-KW Diode Laser. Deposition was made under inert atmosphere by backfilling the chamber with Ar until the O_2 levels were < 10 ppm. After the deposition of four layers, subsequent layers were not deposited since it was hypothesized in the previous work³ that, starting with the fifth layer, there is no change in the first layer. To also investigate the effect of cyclic transformations and the cooling rates on the builds, two wrought Ti-6Al-4V samples were subjected to thermal cycling in a Gleeble thermomechanical simulator. The thermal cycles were obtained by creating a thermal model using simulation of additive manufacturing process (SAMP), a commercial software developed at Applied Optimization. After thermal cycling, the samples were cooled to room temperature using two cooling rates

- i. 200°C/s by quenching with ice water and He,
- ii. 7°C/s by air cooling.

Following deposition, the samples were sectioned in the middle cutting with a low-speed saw with a coolant and then cold-mounted in epoxy to minimize

the temperature rise in the builds. Following mounting, the samples were polished using standard metallographic techniques and then the final polishing was done using a 0.05- μm colloidal silica solution in a Buehler VibroMet2 vibratory polisher. The samples were etched for 20 s with Kroll's reagent. Optical microscopy was done in a Leica 100 microscope. Following optical microscopy, the samples were re-polished with colloidal silica again for 6 h to remove the etched surface to carry out orientation imaging microscopy (OIM) using electron backscatter diffraction (EBSD). EBSD was performed using a JEOL 6500 SEM with an accelerating voltage of 20 kV and probe current of 4 nA. A step size of 0.5 μm was used in an attempt to index the beta phase.

RESULTS AND DISCUSSIONS

Microstructure Evolution During Additive Manufacturing

The optical micrographs are presented in Fig. 2a and b. The microstructure in the single layered build shows columnar prior beta grain morphology at the bottom and an equiaxed grain structure at the top (shown in Fig. 2a) which remains fully equiaxed in the ends of the builds. This gradient in the prior beta grain morphology in the microstructure is hypothesized to be a result of the G versus R varying continuously during the build.¹⁶ In both the columnar and the equiaxed grains, the microstructure after the deposition of the first layer is predominantly α' Martensite. The average size of the equiaxed prior β grains was close to 95 μm and the columnar prior β grains (marked in Fig. 1) was close to 800 μm . The build height of the individual layer is 500 μm and hence it is clear that the grains have developed epitaxially from the substrate towards the surface. The effect of a large columnar prior beta grain size is important from a texture standpoint since it has been shown that larger prior beta grains tend to experience stronger transformation texture than smaller prior beta grains.¹⁷ The formation of α' Martensite has been well established in the selective laser melting process due to the rapid cooling rates involved,¹⁸ and it is indeed possible that α' could form in the first layer of the build. The room-temperature β phase in this case could not be indexed using high-resolution EBSD. However, the presence of β at room temperature has been observed using TEM during quenching at 500 K/s.³ On the deposition of the second layer, the top surface of the first layer is expected to melt. If this occurs, then epitaxial growth of the prior beta grain boundary from the bottom layer should be evident, which is what has been observed from optical microscopy analysis as shown in Fig. 2b. This observation has been previously documented.^{2,3} The inverse pole figures obtained from electron backscattered diffraction for all the builds are presented in Fig. 3a–d. Figure 3a shows the microstructure obtained after the deposition of the first layer. Due to the rapid

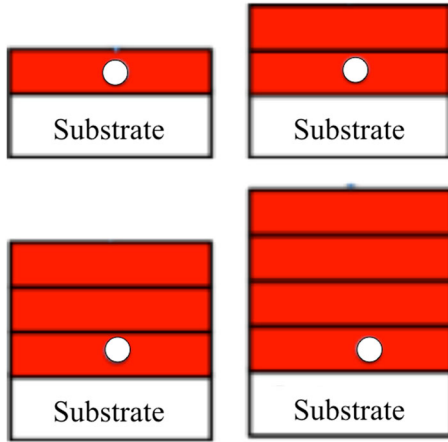


Fig. 1. Schematic of the regions (marked with a white circle) where the microstructure is analyzed.

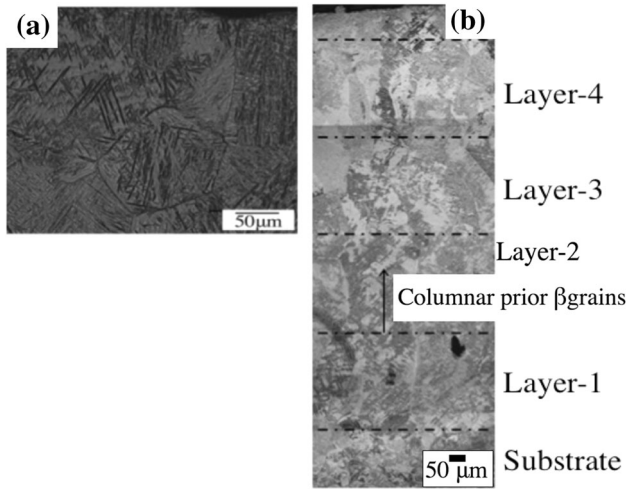


Fig. 2. (a) The equiaxed prior beta grains at the surface of the deposit with martensitic microstructure; (b) the epitaxial growth of the columnar grains throughout the deposit after the deposition of four layers. The builds are sectioned along the direction.

cooling rates experienced, the build forms a martensitic microstructure. It is pertinent to mention that the Martensite laths grow coarser with the deposition on additional layers, as shown in Fig. 3b and c. Figure 3b and c shows the inverse pole figures after the deposition of two and three layers, respectively. After the deposition of layer 4 (shown in Fig. 3d), the microstructure transforms from Martensite to a basketweave and colony microstructure. This confirms that the microstructure in the first layer breaks down with the deposition of further layers as previously shown.^{3,5}

Thermal Cycling Using Gleeble

The thermal cycles that the samples were subjected to are shown in Fig. 4. Thermal cycling in the Gleeble of the sample that had been cooled at 200°C/s

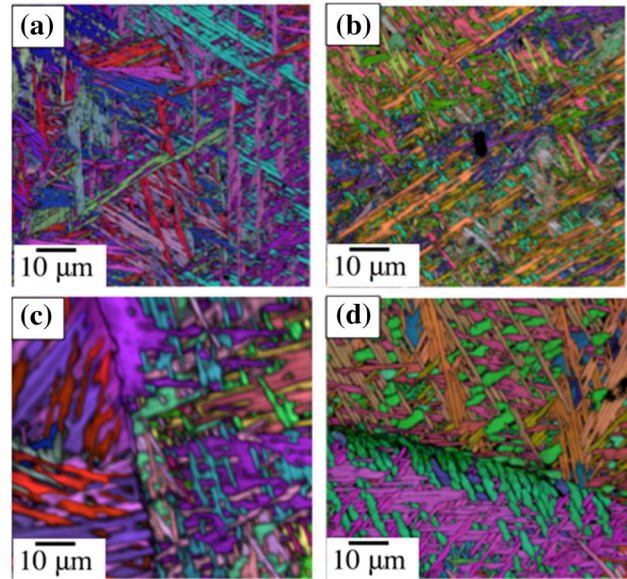


Fig. 3. EBSD scans of deposits after the deposition of (a) one layer, (b) two layers, (c) three layers, and (d) four layers.

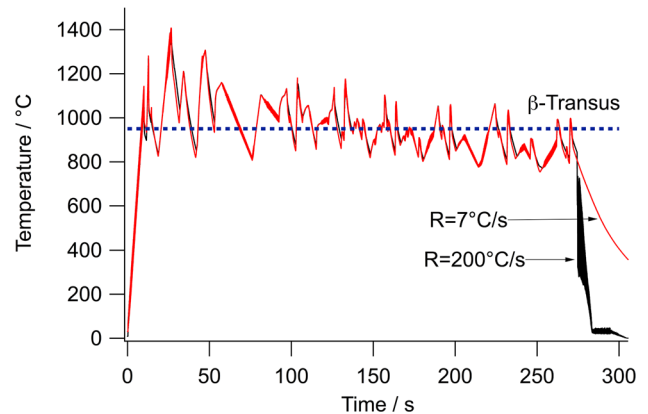


Fig. 4. Thermal cycles simulated using a Gleeble thermo mechanical simulator.

showed a martensitic microstructure while the sample cooled at 7°C/s showed a colony + basket weave microstructure. The main aim of the thermal cycling experiment was to understand whether prolonged thermal cycling had an effect on the final microstructure or whether the final microstructure was a result of the cooling rate from the final beta transus. If prolonged thermal cycling (both above and below the beta transus) had a predominant effect on the microstructure, then the two samples cooled at different cooling rates should have had similar microstructures. The optical microstructures are shown in Fig. 5a and b. Figure 5a, which was quenched, shows a martensitic microstructure, whereas Fig. 5b, which experienced slow cooling, shows a colony and a basket weave microstructure. The fact that the microstructure is different proves that the microstructure evolution in additive

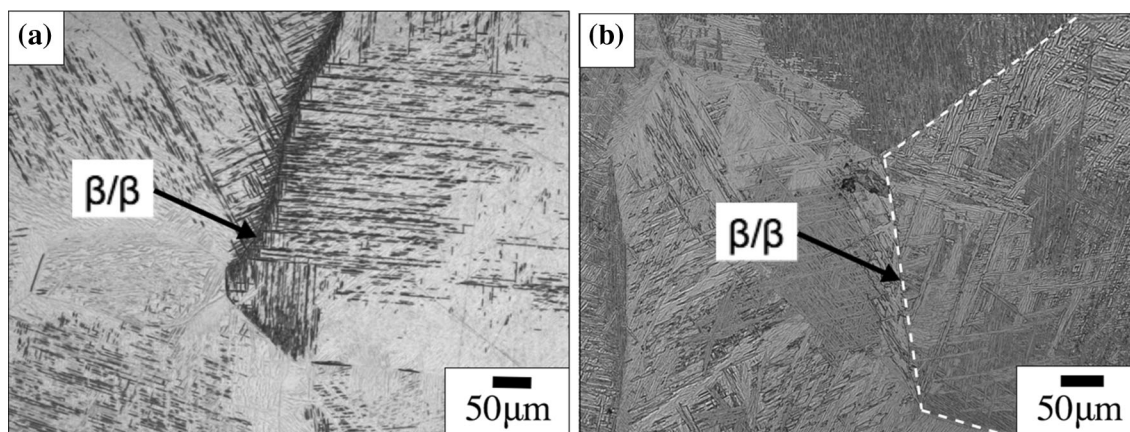


Fig. 5. Optical micrographs of samples after thermal cycling in the Gleeble. (a) Rapidly quenched, (b) slow cooled.

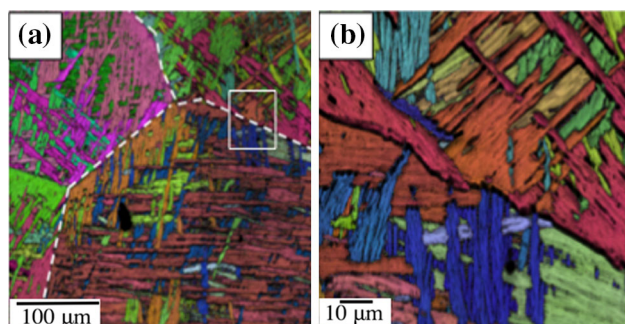


Fig. 6. EBSD images of samples after thermal cycling in the Gleeble. (a) Lower magnification, (b) higher magnification showing the presence of a colony microstructure + basket-weave microstructure.

manufacturing is controlled by the final cooling rate experienced by the build from the Beta transus and the thermal cycling below beta transus may have only a minimal effect. Thus, it is not surprising that, by maintaining the build temperature above the β transus, it is possible to obtain a uniform basket weave microstructure.² For further analysis, EBSD was performed on the sample cooled at 7°C/s to analyze the impact of the slow cooling on the texture. The inverse pole figure maps are presented in Fig. 6a and b. However, more in situ characterization is necessary to validate the above hypothesis.

Texture Evolution as a Function of Build Height

Texture analysis was performed on the samples with a single layer and with four layers along with the samples subjected to thermal cycling in the Gleeble. Figure 7a–c shows the orientation distribution functions (ODFs) obtained from (a) after the deposition of one layer and (b) subsequent deposition of 3 layers (a total of 4 layers), and (c) from the sample that was cooled at 7°C/s after Gleeble simulation. An ODF shows the probability of finding an orientation in the Euler space. Interested readers can find a more comprehensive description on ODF

elsewhere.¹⁹ The texture after the deposition of one layer shows the presence of a strong $\{90^\circ, 90^\circ, 0^\circ\}$, which is associated with the formation of Martensite.¹⁰ The texture of the first layer after the deposition of the fourth layer, which has a basket-weave + colony microstructure, shows a weak $\{90^\circ, 30^\circ, 0^\circ\}$ texture. This means that the $\{0001\}$ basal planes are oriented at an angle of 30° parallel to the direction of building or the Z axis of the build. These textures have been previously documented and reported during heat treatment,^{9,10,13,20} The texture in the sample cooled at 7°C/s after Gleeble simulation also showed a similar $\{90^\circ, 30^\circ, 0^\circ\}$, but the texture showed a strength of 36 times random as against 22 times random for the previous case. The presence of the transformation texture in the builds inspected previously could not be detected since the texture was obtained from the large area scans spanning the total length of the build,^{14,15} The change in the texture obtained after the deposition of four layers is hypothesized to occur as a result of the change in the mechanism of phase transformation.

Variant Selection and Texture in Titanium Alloys

The evolution of transformation texture during additive manufacturing can be rationalized by understanding the mechanism of variant selection. As stated previously, the BCC to HCP transformation occurs with a specific Burger's orientation relationship. During diffusion controlled phase transformation of the α variant, which nucleates on the grain boundary of the prior β grains with a common $\{110\}$ pole, the α will grow with a common $\{0001\}$ pole oriented parallel to the common $\{110\}$ pole. Consequently, the two variants will have their $\langle 11\bar{2}0 \rangle_\alpha$ rotated by 10° .⁸ This sharing of common basal poles leads to a strong alpha transformation texture. To illustrate the above hypothesis, selected grains were extracted to examine the orientation of the α and the Martensite laths formed and are shown in Figs. 8 and 9. During diffusional transformation,

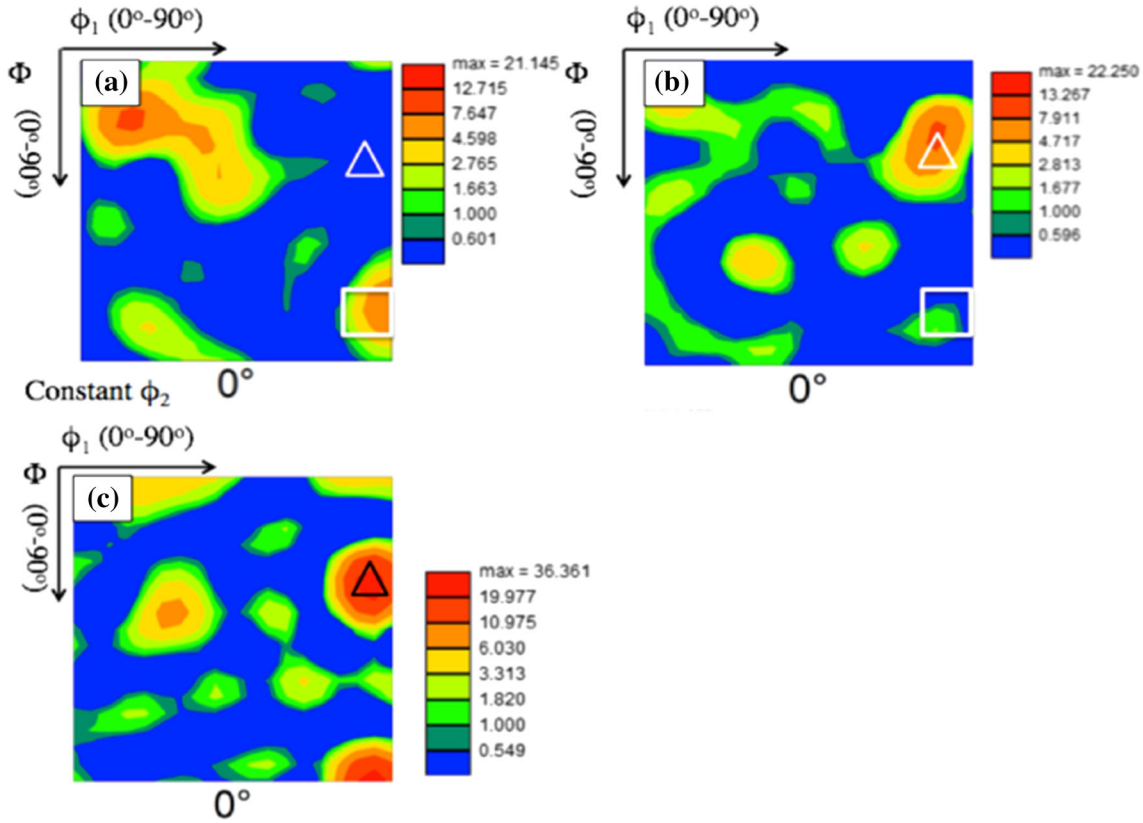


Fig. 7. ODFs of the deposits after deposition of (a) one layer and (b) four layers, (c) after thermal cycling in the Gleeble and slow-cooled. Note the presence of a strong $(90^\circ, 30^\circ, 0^\circ)$ in the Gleeble-processed samples, and the samples after deposition of four layers.

variant selection takes place to minimize the nucleation energy on the non-Burger's side of the prior beta grain. This occurs by selecting a suitable $\langle 11\bar{2}0 \rangle_{\alpha'}$ || $\langle 111 \rangle_{\alpha}$,^{8,12} Thus, the alpha nuclei possess an orientation with a common basal plane leading to a stronger transformation texture as stated previously. This is exactly what is observed in Fig. 8a and c where the $\{0001\}_{\alpha}$ poles are aligned and the $\langle 11\bar{2}0 \rangle_{\alpha}$ are rotated by 10° . Consequently, the alignment of the basal planes results in the observed $\{90^\circ, 30^\circ, 0^\circ\}$ texture.

However, in the case of the Martensite laths obtained after the deposition of the first layer, Fig. 9a and b shows that the $\langle 11\bar{2}0 \rangle_{\alpha}$ directions are aligned but the $\{0001\}_{\alpha}$ are rotated by 60° , thereby resulting in a weaker $\{90^\circ, 30^\circ, 0^\circ\}$ texture. This change in the transformation texture indicates that the laths are Martensite and not α . It has been reported that, during martensitic transformations in titanium alloys, the α' laths choose variants in such a way as to self-accommodate the shape strains,^{10,11} The shape strain arises from the fact that the formation of Martensite may result in a large volume change. Using the phenomenological theory of martensitic transformations, the shape strains were calculated for a number of combinations of variants, and it was reported that the maximum shape strain accommodation was observed for three variants in

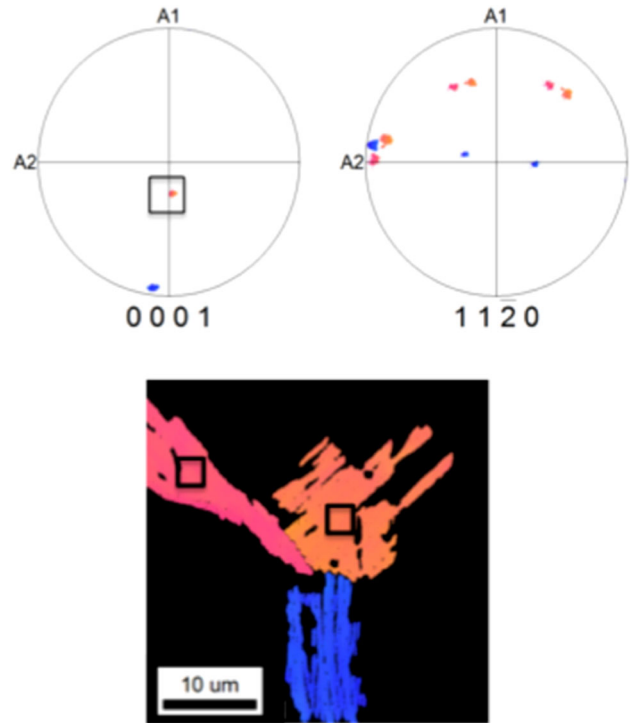


Fig. 8. The orientation relationship between two adjacent laths after thermal cycling in the Gleeble and slow cooling sharing a common (0001) pole which contributes to texture strengthening.

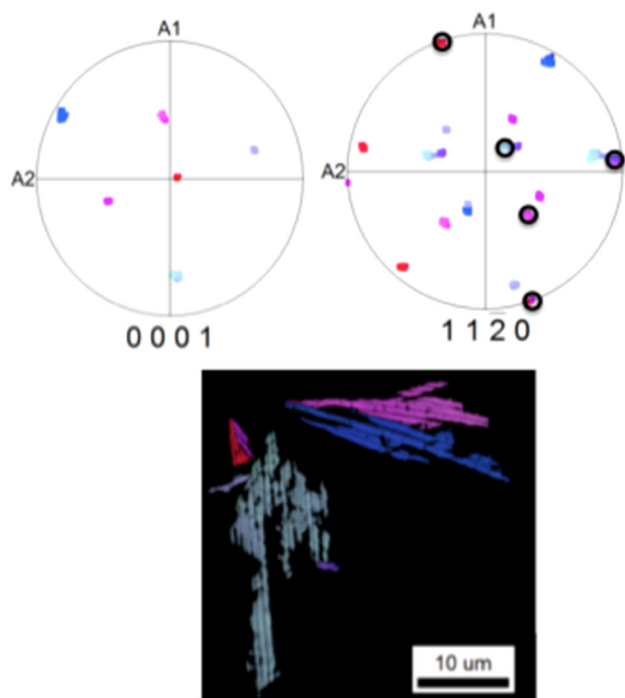


Fig. 9. The orientation relationship between two adjacent laths in the sample after deposition of a single layer showing that they share a common $\langle 1120 \rangle$ instead of a common $\langle 0001 \rangle$ pole, contributing to a decrease in the strength of the $\langle 0001 \rangle$ texture.

two kinds of clusters.¹¹ The first cluster consisted of three α' variants misoriented 63.26° around the $\langle 10553 \rangle_{\alpha'}$ axis, while the second cluster consists of three variants misoriented by 60° around the $\langle 1120 \rangle_{\alpha'}$. These clusters were shown to accommodate shape strain produced by the martensitic transformation.^{10,11,21} Thus, the $\{0001\}_{\alpha}$ texture strength is expected to get weaker with an increase in the cooling rate promoting a martensitic transformation. This shows the importance of the cooling rate from above the beta transus on the texture in AM parts. Thus, attempts to control the cooling rate of the AM parts may offer significant opportunities to control the texture by tailoring the microstructure.

SUMMARY

The texture evolution of LMD Ti-6Al-4V has been studied as a function of the number of layers deposited and the effect of deposition of subsequent layers on the previous layers. The presence of an equiaxed microstructure was observed at the surface of the single-layered deposits while the bottom of the layer close to the substrate remains columnar. This is attributed to the effect of changing G versus R where the columnar to equiaxed transition occurs as previously stated. Characterization of the builds using optical microscopy and EBSD shows the presence of α' Martensite in the single-layer deposits which transforms to a colony and a basket-weave microstructure after the deposition of the fourth layer. The transformation from the α' Martensite to

the colony and basket-weave microstructure occurred as a result of the multiple thermal cycles experienced by the build during subsequent depositions. This transformation also increases the strength of the basal texture as a result of the lower cooling rate experienced as the build cools from the beta transus. Thus, by holding the build above the beta transus during deposition, and by inducing variant selection by promoting diffusional products during cooling, thereby fabricating parts with a strong basal texture, leads to the enhancement of texture-induced strengthening.

ACKNOWLEDGEMENTS

The authors would like to thank the US Navy Small Business Innovation Research program for financial support. This Research was sponsored the U.S. Department of Energy, Office of Energy Efficiency and Renewable Energy, Advanced Manufacturing Office, under contract DE-AC05-00OR22725 with UT-Battelle, LLC. This research at the Oak Ridge National Laboratory's High Temperature Materials Laboratory was sponsored by the U.S. Department of Energy, Office of Energy Efficiency and Renewable Energy, Vehicle Technologies Program.

REFERENCES

1. I. Lonardelli, N. Gey, H.-R. Wenk, M. Humbert, S.C. Vogel, and L. Lutterotti, *Acta Mater.* 55, 5718 (2007).
2. K.T. Makiewicz, Masters Dissertation, The Ohio State University, 2013.
3. S.M. Kelly, Doctoral Dissertation, Virginia Polytechnic Institute and State University, 2002.
4. P.A. Kobryn, and S.L. Semiatin, in *Solid Freeform Fabrication Proceedings*, vol. 6, Austin, 2001.
5. A.W. Prabhu, Masters Dissertation, The Ohio State University, 2014.
6. M.R. Bache, W.J. Evans, B. Suddell, and F.R.M. Herrouin, *Int. J. Fatigue* 23, 153 (2001).
7. B. Baufeld, O. Van der Biest, and S. Dillien, *Metall. Trans. A* 41A, 1917 (2010).
8. D. Bhattacharyya, G.B. Viswanathan, R. Denkenberger, D. Furrer, and H.L. Fraser, *Acta Mater.* 51, 4679 (2003).
9. G.C. Obasi, S. Biroscu, J.Q. da Fonseca, and M. Preuss, *Acta Mater.* 60, 1048 (2012).
10. H. Beladi, Q. Chao, and G.S. Rohrer, *Acta Mater.* 80, 478 (2014).
11. S.C. Wang, M. Aindow, and M.J. Starink, *Acta Mater.* 51, 2485 (2003).
12. E. Lee, R. Banerjee, S. Kar, D. Bhattacharyya, and H.L. Fraser, *Philos. Mag.* 87, 3615 (2007).
13. G.C. Obasi, R.J. Moat, D.G. Leo Prakash, W. Kockelmann, J.Q. da Fonseca, and M. Preuss, *Acta Mater.* 60, 7169 (2012).
14. S.S. Al-Bermani, M.L. Blackmore, W. Zhang, and I. Todd, *Metall. Trans. A* 41A, 3422 (2010).
15. A.A. Antonysamy, P.B. Prangnell, and J. Meyer, *Mater. Sci. Forum* 706, 205 (2012).
16. S. Bontha, N.W. Klingbeil, P.A. Kobryn, and H.L. Fraser, *J. Mater. Process. Technol.* 178, 135 (2006).
17. G.C. Obasi, D.G. Leo Prakash, J.Q. da Fonseca, and M. Preuss, *Acta Mater.* 60, 6013 (2012).
18. L. Thijs, F. Verhaeghe, T. Craeghs, J. Van Humbeeck, and J.P. Kruth, *Acta Mater.* 58, 3303 (2010).
19. V. Randle and O. Engler, *Introduction to Texture Analysis: Macrotexture, Microtexture and Orientation Mapping* (Boca Raton: CRC Press, 2000).
20. N. Stanford and P.S. Bate, *Acta Mater.* 52, 5215 (2004).
21. M. Simonelli, Y.Y. Tse, and C. Tuck, *Metall. Trans. A* 45A, 2863 (2014).